Chapter 2

Image formation

R. Szeliski, *Computer Vision: Algorithms and Applications*, Texts in Computer Science,
DOI 10.1007/978-1-84882-935-0_2, © Springer-Verlag London Limited 2011

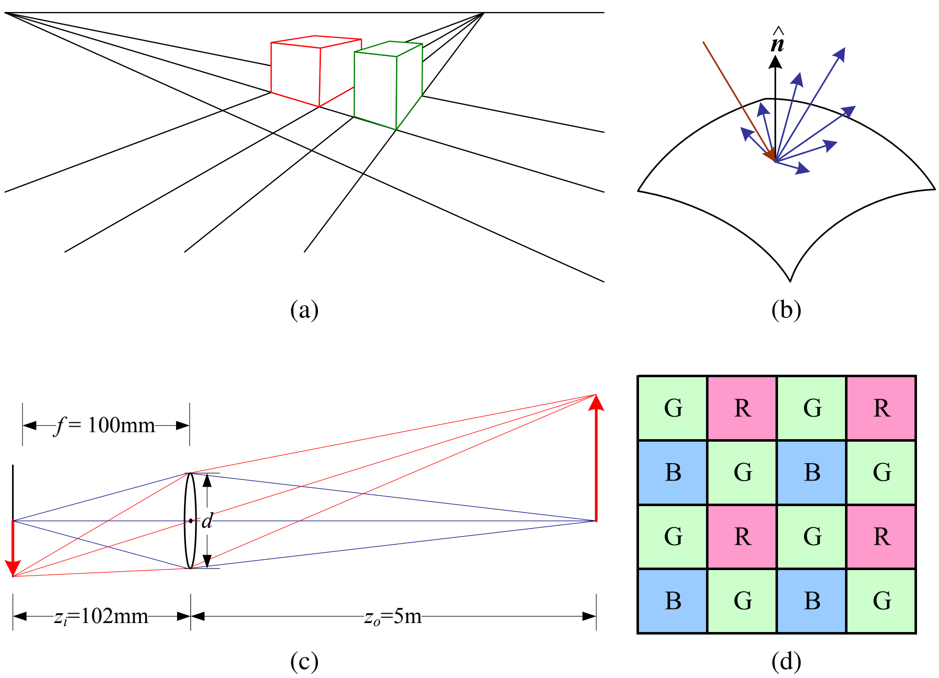

Figure 2.1 A few components of the image formation process: (a) perspective projection; (b) light scattering when hitting a surface; (c) lens optics; (d) Bayer color filter array.

Before we can intelligently analyze and manipulate images, we need to establish a vocabulary for describing the geometry of a scene. We also need to understand the image formation process that produced a particular image given a set of lighting conditions, scene geometry, surface properties, and camera optics. In this chapter, we present a simplified model of such an image formation process.

Section 2.1 introduces the basic geometric primitives used throughout the book (points, lines, and planes) and the *geometric* transformations that project these 3D quantities into 2D image features (Figure 2.1a). Section 2.2 describes how lighting, surface properties (Figure 2.1b), and camera *optics* (Figure 2.1c) interact in order to produce the color values that fall onto the image sensor. Section 2.3 describes how continuous color images are turned into discrete digital *samples* inside the image sensor (Figure 2.1d) and how to avoid (or at least characterize) sampling deficiencies, such as aliasing.

The material covered in this chapter is but a brief summary of a very rich and deep set of topics, traditionally covered in a number of separate fields. A more thorough introduction to the geometry of points, lines, planes, and projections can be found in textbooks on multi-view geometry (Hartley and Zisserman 2004; Faugeras and Luong 2001) and computer graphics (Foley, van Dam, Feiner *et al.* 1995). The image formation (synthesis) process is traditionally taught as part of a computer graphics curriculum (Foley, van Dam, Feiner *et al.* 1995; Glassner 1995; Watt 1995; Shirley 2005) but it is also studied in physics-based computer vision (Wolff, Shafer, and Healey 1992a). The behavior of camera lens systems is studied in optics (Möller 1988; Hecht 2001; Ray 2002). Two good books on color theory are (Wyszecki and Stiles 2000; Healey and Shafer 1992), with (Livingstone 2008) providing a more fun and informal introduction to the topic of color perception. Topics relating to sampling and aliasing are covered in textbooks on signal and image processing (Crane 1997; Jähne 1997; Oppenheim and Schafer 1996; Oppenheim, Schafer, and Buck 1999; Pratt 2007; Russ 2007; Burger and Burge 2008; Gonzales and Woods 2008).

A note to students: If you have already studied computer graphics, you may want to skim the material in Section 2.1, although the sections on projective depth and object-centered projection near the end of Section 2.1.5 may be new to you. Similarly, physics students (as well as computer graphics students) will mostly be familiar with Section 2.2. Finally, students with a good background in image processing will already be familiar with sampling issues (Section 2.3) as well as some of the material in Chapter 3.

2.1 Geometric primitives and transformations

In this section, we introduce the basic 2D and 3D primitives used in this textbook, namely points, lines, and planes. We also describe how 3D features are projected into 2D features. More detailed descriptions of these topics (along with a gentler and more intuitive introduction) can be found in textbooks on multiple-view geometry (Hartley and Zisserman 2004; Faugeras and Luong 2001).

2.1.1 Geometric primitives

Geometric primitives form the basic building blocks used to describe three-dimensional shapes. In this section, we introduce points, lines, and planes. Later sections of the book discuss

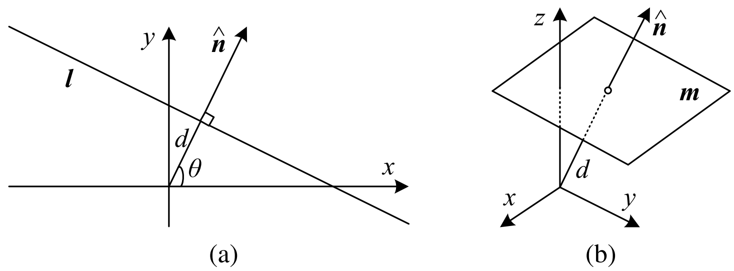

Figure 2.2 (a) 2D line equation and (b) 3D plane equation, expressed in terms of the normal $\hat{\boldsymbol{n}}$ and distance to the origin d.

curves (Sections 5.1 and 11.2), surfaces (Section 12.3), and volumes (Section 12.5).

2D points. 2D points (pixel coordinates in an image) can be denoted using a pair of values, $\boldsymbol{x} = (x, y) \in \mathcal{R}^2$, or alternatively,

$$\boldsymbol{x} = \begin{bmatrix} x \\ y \end{bmatrix}. \tag{2.1}$$

(As stated in the introduction, we use the $(x_1, x_2, \ldots)$ notation to denote column vectors.)

2D points can also be represented using *homogeneous coordinates*, $\tilde{\boldsymbol{x}} = (\tilde{x}, \tilde{y}, \tilde{w}) \in \mathcal{P}^2$, where vectors that differ only by scale are considered to be equivalent. $\mathcal{P}^2 = \mathcal{R}^3 - (0, 0, 0)$ is called the 2D *projective space*.

A homogeneous vector $\tilde{\boldsymbol{x}}$ can be converted back into an *inhomogeneous* vector $\boldsymbol{x}$ by dividing through by the last element $\tilde{w}$, i.e.,

$$\tilde{\boldsymbol{x}} = (\tilde{x}, \tilde{y}, \tilde{w}) = \tilde{w}(x, y, 1) = \tilde{w}\bar{\boldsymbol{x}}, \tag{2.2}$$

where $\bar{\boldsymbol{x}} = (x, y, 1)$ is the *augmented vector*. Homogeneous points whose last element is $\tilde{w} = 0$ are called *ideal points* or *points at infinity* and do not have an equivalent inhomogeneous representation.

2D lines. 2D lines can also be represented using homogeneous coordinates $\tilde{\boldsymbol{l}} = (a, b, c)$. The corresponding *line equation* is

$$\bar{\boldsymbol{x}} \cdot \tilde{\boldsymbol{l}} = ax + by + c = 0. \tag{2.3}$$

We can normalize the line equation vector so that $\boldsymbol{l} = (\hat{n}_x, \hat{n}_y, d) = (\hat{\boldsymbol{n}}, d)$ with $\|\hat{\boldsymbol{n}}\| = 1$. In this case, $\hat{\boldsymbol{n}}$ is the *normal vector* perpendicular to the line and d is its distance to the origin (Figure 2.2). (The one exception to this normalization is the *line at infinity* $\tilde{\boldsymbol{l}} = (0, 0, 1)$, which includes all (ideal) points at infinity.)

We can also express $\hat{\boldsymbol{n}}$ as a function of rotation angle θ, $\hat{\boldsymbol{n}} = (\hat{n}_x, \hat{n}_y) = (\cos\theta, \sin\theta)$ (Figure 2.2a). This representation is commonly used in the *Hough transform* line-finding algorithm, which is discussed in Section 4.3.2. The combination (θ, d) is also known as *polar coordinates*.

When using homogeneous coordinates, we can compute the intersection of two lines as

$$\tilde{\boldsymbol{x}} = \tilde{\boldsymbol{l}}_1 \times \tilde{\boldsymbol{l}}_2, \tag{2.4}$$

where $\times$ is the cross product operator. Similarly, the line joining two points can be written as

$$\tilde{\boldsymbol{l}} = \tilde{\boldsymbol{x}}_1 \times \tilde{\boldsymbol{x}}_2. \tag{2.5}$$

When trying to fit an intersection point to multiple lines or, conversely, a line to multiple points, least squares techniques (Section 6.1.1 and Appendix A.2) can be used, as discussed in Exercise 2.1.

2D conics. There are other algebraic curves that can be expressed with simple polynomial homogeneous equations. For example, the *conic sections* (so called because they arise as the intersection of a plane and a 3D cone) can be written using a *quadric* equation

$$\tilde{\boldsymbol{x}}^T \boldsymbol{Q} \tilde{\boldsymbol{x}} = 0. \tag{2.6}$$

Quadric equations play useful roles in the study of multi-view geometry and camera calibration (Hartley and Zisserman 2004; Faugeras and Luong 2001) but are not used extensively in this book.

3D points. Point coordinates in three dimensions can be written using inhomogeneous coordinates $\boldsymbol{x} = (x, y, z) \in \mathcal{R}^3$ or homogeneous coordinates $\tilde{\boldsymbol{x}} = (\tilde{x}, \tilde{y}, \tilde{z}, \tilde{w}) \in \mathcal{P}^3$. As before, it is sometimes useful to denote a 3D point using the augmented vector $\bar{\boldsymbol{x}} = (x, y, z, 1)$ with $\tilde{\boldsymbol{x}} = \tilde{w}\bar{\boldsymbol{x}}$.

3D planes. 3D planes can also be represented as homogeneous coordinates $\tilde{\boldsymbol{m}} = (a, b, c, d)$ with a corresponding plane equation

$$\bar{\boldsymbol{x}} \cdot \tilde{\boldsymbol{m}} = ax + by + cz + d = 0. \tag{2.7}$$

We can also normalize the plane equation as $\boldsymbol{m} = (\hat{n}_x, \hat{n}_y, \hat{n}_z, d) = (\hat{\boldsymbol{n}}, d)$ with $\|\hat{\boldsymbol{n}}\| = 1$. In this case, $\hat{\boldsymbol{n}}$ is the *normal vector* perpendicular to the plane and d is its distance to the origin (Figure 2.2b). As with the case of 2D lines, the *plane at infinity* $\tilde{\boldsymbol{m}} = (0, 0, 0, 1)$, which contains all the points at infinity, cannot be normalized (i.e., it does not have a unique normal or a finite distance).

We can express $\hat{\boldsymbol{n}}$ as a function of two angles (θ, ϕ),

$$\hat{\boldsymbol{n}} = (\cos\theta\cos\phi, \sin\theta\cos\phi, \sin\phi), \tag{2.8}$$

i.e., using *spherical coordinates*, but these are less commonly used than polar coordinates since they do not uniformly sample the space of possible normal vectors.

3D lines. Lines in 3D are less elegant than either lines in 2D or planes in 3D. One possible representation is to use two points on the line, $(\boldsymbol{p}, \boldsymbol{q})$. Any other point on the line can be expressed as a linear combination of these two points

$$\boldsymbol{r} = (1 - \lambda)\boldsymbol{p} + \lambda\boldsymbol{q}, \tag{2.9}$$

as shown in Figure 2.3. If we restrict $0 \le \lambda \le 1$, we get the *line segment* joining $\boldsymbol{p}$ and $\boldsymbol{q}$.

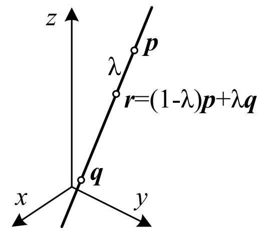

Figure 2.3 3D line equation, $\boldsymbol{r} = (1 - \lambda)\boldsymbol{p} + \lambda\boldsymbol{q}$.

If we use homogeneous coordinates, we can write the line as

$$\tilde{\boldsymbol{r}} = \mu\tilde{\boldsymbol{p}} + \lambda\tilde{\boldsymbol{q}}. \tag{2.10}$$

A special case of this is when the second point is at infinity, i.e., $\tilde{\boldsymbol{q}} = (\hat{d}_x, \hat{d}_y, \hat{d}_z, 0) = (\hat{\boldsymbol{d}}, 0)$. Here, we see that $\hat{\boldsymbol{d}}$ is the *direction* of the line. We can then re-write the inhomogeneous 3D line equation as

$$\boldsymbol{r} = \boldsymbol{p} + \lambda\hat{\boldsymbol{d}}. \tag{2.11}$$

A disadvantage of the endpoint representation for 3D lines is that it has too many degrees of freedom, i.e., six (three for each endpoint) instead of the four degrees that a 3D line truly has. However, if we fix the two points on the line to lie in specific planes, we obtain a representation with four degrees of freedom. For example, if we are representing nearly vertical lines, then $z = 0$ and $z = 1$ form two suitable planes, i.e., the (x, y) coordinates in both planes provide the four coordinates describing the line. This kind of two-plane parameterization is used in the *light field* and *Lumigraph* image-based rendering systems described in Chapter 13 to represent the collection of rays seen by a camera as it moves in front of an object. The two-endpoint representation is also useful for representing line segments, even when their exact endpoints cannot be seen (only guessed at).

If we wish to represent all possible lines without bias towards any particular orientation, we can use *Plücker coordinates* (Hartley and Zisserman 2004, Chapter 2; Faugeras and Luong 2001, Chapter 3). These coordinates are the six independent non-zero entries in the 4×4 skew symmetric matrix

$$\boldsymbol{L} = \tilde{\boldsymbol{p}}\tilde{\boldsymbol{q}}^T - \tilde{\boldsymbol{q}}\tilde{\boldsymbol{p}}^T, \tag{2.12}$$

where $\tilde{\boldsymbol{p}}$ and $\tilde{\boldsymbol{q}}$ are *any* two (non-identical) points on the line. This representation has only four degrees of freedom, since $\boldsymbol{L}$ is homogeneous and also satisfies $det(\boldsymbol{L}) = 0$, which results in a quadratic constraint on the Plücker coordinates.

In practice, the minimal representation is not essential for most applications. An adequate model of 3D lines can be obtained by estimating their direction (which may be known ahead of time, e.g., for architecture) and some point within the visible portion of the line (see Section 7.5.1) or by using the two endpoints, since lines are most often visible as finite line segments. However, if you are interested in more details about the topic of minimal line parameterizations, Förstner (2005) discusses various ways to infer and model 3D lines in projective geometry, as well as how to estimate the uncertainty in such fitted models.

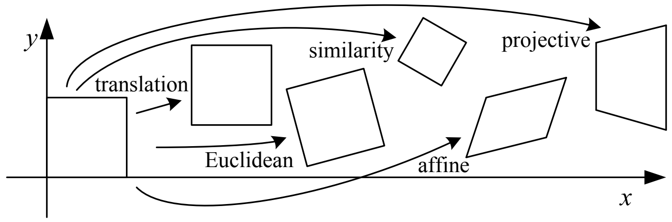

Figure 2.4 Basic set of 2D planar transformations.

3D quadrics. The 3D analog of a conic section is a quadric surface

$$\bar{\boldsymbol{x}}^T \boldsymbol{Q} \bar{\boldsymbol{x}} = 0 \tag{2.13}$$

(Hartley and Zisserman 2004, Chapter 2). Again, while quadric surfaces are useful in the study of multi-view geometry and can also serve as useful modeling primitives (spheres, ellipsoids, cylinders), we do not study them in great detail in this book.

2.1.2 2D transformations

Having defined our basic primitives, we can now turn our attention to how they can be transformed. The simplest transformations occur in the 2D plane and are illustrated in Figure 2.4.

Translation. 2D translations can be written as $\boldsymbol{x}' = \boldsymbol{x} + \boldsymbol{t}$ or

$$\boldsymbol{x}' = \begin{bmatrix} \boldsymbol{I} & \boldsymbol{t} \end{bmatrix} \bar{\boldsymbol{x}} \tag{2.14}$$

where $\boldsymbol{I}$ is the (2×2) identity matrix or

$$\bar{\boldsymbol{x}}' = \begin{bmatrix} \boldsymbol{I} & \boldsymbol{t} \\ \boldsymbol{0}^T & 1 \end{bmatrix} \bar{\boldsymbol{x}} \tag{2.15}$$

where $\boldsymbol{0}$ is the zero vector. Using a 2×3 matrix results in a more compact notation, whereas using a full-rank 3×3 matrix (which can be obtained from the 2×3 matrix by appending a $[\boldsymbol{0}^T \; 1]$ row) makes it possible to chain transformations using matrix multiplication. Note that in any equation where an augmented vector such as $\bar{\boldsymbol{x}}$ appears on both sides, it can always be replaced with a full homogeneous vector $\tilde{\boldsymbol{x}}$.

Rotation + translation. This transformation is also known as *2D rigid body motion* or the *2D Euclidean transformation* (since Euclidean distances are preserved). It can be written as $\boldsymbol{x}' = \boldsymbol{R}\boldsymbol{x} + \boldsymbol{t}$ or

$$\boldsymbol{x}' = \begin{bmatrix} \boldsymbol{R} & \boldsymbol{t} \end{bmatrix} \bar{\boldsymbol{x}} \tag{2.16}$$

where

$$\boldsymbol{R} = \begin{bmatrix} \cos\theta & -\sin\theta \\ \sin\theta & \cos\theta \end{bmatrix} \tag{2.17}$$

is an orthonormal rotation matrix with $\boldsymbol{R}\boldsymbol{R}^T = \boldsymbol{I}$ and $|\boldsymbol{R}| = 1$.

Scaled rotation. Also known as the *similarity transform*, this transformation can be expressed as $\boldsymbol{x}' = s\boldsymbol{R}\boldsymbol{x} + \boldsymbol{t}$ where s is an arbitrary scale factor. It can also be written as

$$\boldsymbol{x}' = \begin{bmatrix} s\boldsymbol{R} & \boldsymbol{t} \end{bmatrix} \bar{\boldsymbol{x}} = \begin{bmatrix} a & -b & t_x \\ b & a & t_y \end{bmatrix} \bar{\boldsymbol{x}}, \tag{2.18}$$

where we no longer require that $a^2 + b^2 = 1$. The similarity transform preserves angles between lines.

Affine. The affine transformation is written as $\boldsymbol{x}' = \boldsymbol{A}\bar{\boldsymbol{x}}$, where $\boldsymbol{A}$ is an arbitrary 2×3 matrix, i.e.,

$$\boldsymbol{x}' = \begin{bmatrix} a_{00} & a_{01} & a_{02} \\ a_{10} & a_{11} & a_{12} \end{bmatrix} \bar{\boldsymbol{x}}. \tag{2.19}$$

Parallel lines remain parallel under affine transformations.

Projective. This transformation, also known as a *perspective transform* or *homography*, operates on homogeneous coordinates,

$$\tilde{\boldsymbol{x}}' = \tilde{\boldsymbol{H}}\tilde{\boldsymbol{x}}, \tag{2.20}$$

where $\tilde{\boldsymbol{H}}$ is an arbitrary 3×3 matrix. Note that $\tilde{\boldsymbol{H}}$ is homogeneous, i.e., it is only defined up to a scale, and that two $\tilde{\boldsymbol{H}}$ matrices that differ only by scale are equivalent. The resulting homogeneous coordinate $\tilde{\boldsymbol{x}}'$ must be normalized in order to obtain an inhomogeneous result $\boldsymbol{x}$, i.e.,

$$x' = \frac{h_{00}x + h_{01}y + h_{02}}{h_{20}x + h_{21}y + h_{22}} \quad \text{and} \quad y' = \frac{h_{10}x + h_{11}y + h_{12}}{h_{20}x + h_{21}y + h_{22}}. \tag{2.21}$$

Perspective transformations preserve straight lines (i.e., they remain straight after the transformation).

Hierarchy of 2D transformations. The preceding set of transformations are illustrated in Figure 2.4 and summarized in Table 2.1. The easiest way to think of them is as a set of (potentially restricted) 3×3 matrices operating on 2D homogeneous coordinate vectors. Hartley and Zisserman (2004) contains a more detailed description of the hierarchy of 2D planar transformations.

The above transformations form a nested set of *groups*, i.e., they are closed under composition and have an inverse that is a member of the same group. (This will be important later when applying these transformations to images in Section 3.6.) Each (simpler) group is a subset of the more complex group below it.

Co-vectors. While the above transformations can be used to transform points in a 2D plane, can they also be used directly to transform a line equation? Consider the homogeneous equation $\tilde{\boldsymbol{l}} \cdot \tilde{\boldsymbol{x}} = 0$. If we transform $\boldsymbol{x}' = \tilde{\boldsymbol{H}}\boldsymbol{x}$, we obtain

$$\tilde{\boldsymbol{l}}' \cdot \tilde{\boldsymbol{x}}' = \tilde{\boldsymbol{l}}'^T \tilde{\boldsymbol{H}}\tilde{\boldsymbol{x}} = (\tilde{\boldsymbol{H}}^T \tilde{\boldsymbol{l}}')^T \tilde{\boldsymbol{x}} = \tilde{\boldsymbol{l}} \cdot \tilde{\boldsymbol{x}} = 0, \tag{2.22}$$

i.e., $\tilde{\boldsymbol{l}}' = \tilde{\boldsymbol{H}}^{-T}\tilde{\boldsymbol{l}}$. Thus, the action of a projective transformation on a *co-vector* such as a 2D line or 3D normal can be represented by the transposed inverse of the matrix, which is equivalent to the *adjoint* of $\tilde{\boldsymbol{H}}$, since projective transformation matrices are homogeneous. Jim

Transformation	Matrix	# DoF	Preserves	Icon
translation	$\begin{bmatrix} \boldsymbol{I} \mid \boldsymbol{t} \end{bmatrix}_{2\times 3}$	2	orientation	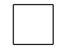
rigid (Euclidean)	$\begin{bmatrix} \boldsymbol{R} \mid \boldsymbol{t} \end{bmatrix}_{2\times 3}$	3	lengths	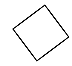
similarity	$\begin{bmatrix} s\boldsymbol{R} \mid \boldsymbol{t} \end{bmatrix}_{2\times 3}$	4	angles	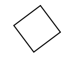
affine	$\begin{bmatrix} \boldsymbol{A} \end{bmatrix}_{2\times 3}$	6	parallelism	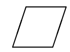
projective	$\begin{bmatrix} \tilde{\boldsymbol{H}} \end{bmatrix}_{3\times 3}$	8	straight lines	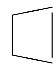

Table 2.1 Hierarchy of 2D coordinate transformations. Each transformation also preserves the properties listed in the rows below it, i.e., similarity preserves not only angles but also parallelism and straight lines. The 2×3 matrices are extended with a third $[\mathbf{0}^T\ 1]$ row to form a full 3×3 matrix for homogeneous coordinate transformations.

Blinn (1998) describes (in Chapters 9 and 10) the ins and outs of notating and manipulating co-vectors.

While the above transformations are the ones we use most extensively, a number of additional transformations are sometimes used.

Stretch/squash. This transformation changes the aspect ratio of an image,

$$\begin{aligned} x' &= s_x x + t_x \\ y' &= s_y y + t_y, \end{aligned}$$

and is a restricted form of an affine transformation. Unfortunately, it does not nest cleanly with the groups listed in Table 2.1.

Planar surface flow. This eight-parameter transformation (Horn 1986; Bergen, Anandan, Hanna *et al.* 1992; Girod, Greiner, and Niemann 2000),

$$\begin{aligned} x' &= a_0 + a_1 x + a_2 y + a_6 x^2 + a_7 xy \\ y' &= a_3 + a_4 x + a_5 y + a_7 x^2 + a_6 xy, \end{aligned}$$

arises when a planar surface undergoes a small 3D motion. It can thus be thought of as a small motion approximation to a full homography. Its main attraction is that it is *linear* in the motion parameters, a_k, which are often the quantities being estimated.

Bilinear interpolant. This eight-parameter transform (Wolberg 1990),

$$\begin{aligned} x' &= a_0 + a_1 x + a_2 y + a_6 xy \\ y' &= a_3 + a_4 x + a_5 y + a_7 xy, \end{aligned}$$

can be used to interpolate the deformation due to the motion of the four corner points of a square. (In fact, it can interpolate the motion of any four non-collinear points.) While

Transformation	Matrix	# DoF	Preserves	Icon
translation	$\left[\begin{array}{c\|c} \boldsymbol{I} & \boldsymbol{t} \end{array}\right]_{3\times 4}$	3	orientation	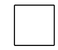
rigid (Euclidean)	$\left[\begin{array}{c\|c} \boldsymbol{R} & \boldsymbol{t} \end{array}\right]_{3\times 4}$	6	lengths	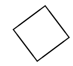
similarity	$\left[\begin{array}{c\|c} s\boldsymbol{R} & \boldsymbol{t} \end{array}\right]_{3\times 4}$	7	angles	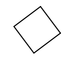
affine	$\left[\begin{array}{c} \boldsymbol{A} \end{array}\right]_{3\times 4}$	12	parallelism	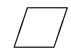
projective	$\left[\begin{array}{c} \tilde{\boldsymbol{H}} \end{array}\right]_{4\times 4}$	15	straight lines	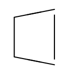

Table 2.2 Hierarchy of 3D coordinate transformations. Each transformation also preserves the properties listed in the rows below it, i.e., similarity preserves not only angles but also parallelism and straight lines. The 3×4 matrices are extended with a fourth $[\mathbf{0}^T\ 1]$ row to form a full 4×4 matrix for homogeneous coordinate transformations. The mnemonic icons are drawn in 2D but are meant to suggest transformations occurring in a full 3D cube.

the deformation is linear in the motion parameters, it does not generally preserve straight lines (only lines parallel to the square axes). However, it is often quite useful, e.g., in the interpolation of sparse grids using splines (Section 8.3).

2.1.3 3D transformations

The set of three-dimensional coordinate transformations is very similar to that available for 2D transformations and is summarized in Table 2.2. As in 2D, these transformations form a nested set of groups. Hartley and Zisserman (2004, Section 2.4) give a more detailed description of this hierarchy.

Translation. 3D translations can be written as $\boldsymbol{x}' = \boldsymbol{x} + \boldsymbol{t}$ or

$$\boldsymbol{x}' = \begin{bmatrix} \boldsymbol{I} & \boldsymbol{t} \end{bmatrix} \bar{\boldsymbol{x}} \tag{2.23}$$

where $\boldsymbol{I}$ is the (3×3) identity matrix and $\mathbf{0}$ is the zero vector.

Rotation + translation. Also known as 3D *rigid body motion* or the 3D *Euclidean transformation*, it can be written as $\boldsymbol{x}' = \boldsymbol{R}\boldsymbol{x} + \boldsymbol{t}$ or

$$\boldsymbol{x}' = \begin{bmatrix} \boldsymbol{R} & \boldsymbol{t} \end{bmatrix} \bar{\boldsymbol{x}} \tag{2.24}$$

where $\boldsymbol{R}$ is a 3×3 orthonormal rotation matrix with $\boldsymbol{R}\boldsymbol{R}^T = \boldsymbol{I}$ and $|\boldsymbol{R}| = 1$. Note that sometimes it is more convenient to describe a rigid motion using

$$\boldsymbol{x}' = \boldsymbol{R}(\boldsymbol{x} - \boldsymbol{c}) = \boldsymbol{R}\boldsymbol{x} - \boldsymbol{R}\boldsymbol{c}, \tag{2.25}$$

where $\boldsymbol{c}$ is the center of rotation (often the camera center).

Compactly parameterizing a 3D rotation is a non-trivial task, which we describe in more detail below.

Scaled rotation. The 3D *similarity transform* can be expressed as $\boldsymbol{x}' = s\boldsymbol{R}\boldsymbol{x} + \boldsymbol{t}$ where s is an arbitrary scale factor. It can also be written as

$$\boldsymbol{x}' = \begin{bmatrix} s\boldsymbol{R} & \boldsymbol{t} \end{bmatrix} \bar{\boldsymbol{x}}. \tag{2.26}$$

This transformation preserves angles between lines and planes.

Affine. The affine transform is written as $\boldsymbol{x}' = \boldsymbol{A}\bar{\boldsymbol{x}}$, where $\boldsymbol{A}$ is an arbitrary 3×4 matrix, i.e.,

$$\boldsymbol{x}' = \begin{bmatrix} a_{00} & a_{01} & a_{02} & a_{03} \\ a_{10} & a_{11} & a_{12} & a_{13} \\ a_{20} & a_{21} & a_{22} & a_{23} \end{bmatrix} \bar{\boldsymbol{x}}. \tag{2.27}$$

Parallel lines and planes remain parallel under affine transformations.

Projective. This transformation, variously known as a *3D perspective transform*, *homography*, or *collineation*, operates on homogeneous coordinates,

$$\tilde{\boldsymbol{x}}' = \tilde{\boldsymbol{H}}\tilde{\boldsymbol{x}}, \tag{2.28}$$

where $\tilde{\boldsymbol{H}}$ is an arbitrary 4×4 homogeneous matrix. As in 2D, the resulting homogeneous coordinate $\tilde{\boldsymbol{x}}'$ must be normalized in order to obtain an inhomogeneous result $\boldsymbol{x}$. Perspective transformations preserve straight lines (i.e., they remain straight after the transformation).

2.1.4 3D rotations

The biggest difference between 2D and 3D coordinate transformations is that the parameterization of the 3D rotation matrix $\boldsymbol{R}$ is not as straightforward but several possibilities exist.

Euler angles

A rotation matrix can be formed as the product of three rotations around three cardinal axes, e.g., x, y, and z, or x, y, and x. This is generally a bad idea, as the result depends on the order in which the transforms are applied. What is worse, it is not always possible to move smoothly in the parameter space, i.e., sometimes one or more of the Euler angles change dramatically in response to a small change in rotation.[1] For these reasons, we do not even give the formula for Euler angles in this book—interested readers can look in other textbooks or technical reports (Faugeras 1993; Diebel 2006). Note that, in some applications, if the rotations are known to be a set of uni-axial transforms, they can always be represented using an explicit set of rigid transformations.

Axis/angle (exponential twist)

A rotation can be represented by a rotation axis $\hat{\boldsymbol{n}}$ and an angle θ, or equivalently by a 3D vector $\boldsymbol{\omega} = \theta\hat{\boldsymbol{n}}$. Figure 2.5 shows how we can compute the equivalent rotation. First, we project the vector $\boldsymbol{v}$ onto the axis $\hat{\boldsymbol{n}}$ to obtain

$$\boldsymbol{v}_{\parallel} = \hat{\boldsymbol{n}}(\hat{\boldsymbol{n}} \cdot \boldsymbol{v}) = (\hat{\boldsymbol{n}}\hat{\boldsymbol{n}}^T)\boldsymbol{v}, \tag{2.29}$$

[1] In robotics, this is sometimes referred to as *gimbal lock*.

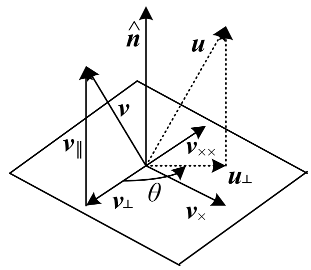

Figure 2.5 Rotation around an axis $\hat{\boldsymbol{n}}$ by an angle θ.

which is the component of $\boldsymbol{v}$ that is not affected by the rotation. Next, we compute the perpendicular residual of $\boldsymbol{v}$ from $\hat{\boldsymbol{n}}$,

$$\boldsymbol{v}_\perp = \boldsymbol{v} - \boldsymbol{v}_\parallel = (\boldsymbol{I} - \hat{\boldsymbol{n}}\hat{\boldsymbol{n}}^T)\boldsymbol{v}. \tag{2.30}$$

We can rotate this vector by $90°$ using the cross product,

$$\boldsymbol{v}_\times = \hat{\boldsymbol{n}} \times \boldsymbol{v} = [\hat{\boldsymbol{n}}]_\times \boldsymbol{v}, \tag{2.31}$$

where $[\hat{\boldsymbol{n}}]_\times$ is the matrix form of the cross product operator with the vector $\hat{\boldsymbol{n}} = (\hat{n}_x, \hat{n}_y, \hat{n}_z)$,

$$[\hat{\boldsymbol{n}}]_\times = \begin{bmatrix} 0 & -\hat{n}_z & \hat{n}_y \\ \hat{n}_z & 0 & -\hat{n}_x \\ -\hat{n}_y & \hat{n}_x & 0 \end{bmatrix}. \tag{2.32}$$

Note that rotating this vector by another $90°$ is equivalent to taking the cross product again,

$$\boldsymbol{v}_{\times\times} = \hat{\boldsymbol{n}} \times \boldsymbol{v}_\times = [\hat{\boldsymbol{n}}]^2_\times \boldsymbol{v} = -\boldsymbol{v}_\perp,$$

and hence

$$\boldsymbol{v}_\parallel = \boldsymbol{v} - \boldsymbol{v}_\perp = \boldsymbol{v} + \boldsymbol{v}_{\times\times} = (\boldsymbol{I} + [\hat{\boldsymbol{n}}]^2_\times)\boldsymbol{v}.$$

We can now compute the in-plane component of the rotated vector $\boldsymbol{u}$ as

$$\boldsymbol{u}_\perp = \cos\theta \boldsymbol{v}_\perp + \sin\theta \boldsymbol{v}_\times = (\sin\theta[\hat{\boldsymbol{n}}]_\times - \cos\theta[\hat{\boldsymbol{n}}]^2_\times)\boldsymbol{v}.$$

Putting all these terms together, we obtain the final rotated vector as

$$\boldsymbol{u} = \boldsymbol{u}_\perp + \boldsymbol{v}_\parallel = (\boldsymbol{I} + \sin\theta[\hat{\boldsymbol{n}}]_\times + (1-\cos\theta)[\hat{\boldsymbol{n}}]^2_\times)\boldsymbol{v}. \tag{2.33}$$

We can therefore write the rotation matrix corresponding to a rotation by θ around an axis $\hat{\boldsymbol{n}}$ as

$$\boldsymbol{R}(\hat{\boldsymbol{n}}, \theta) = \boldsymbol{I} + \sin\theta[\hat{\boldsymbol{n}}]_\times + (1-\cos\theta)[\hat{\boldsymbol{n}}]^2_\times, \tag{2.34}$$

which is known as *Rodriguez's formula* (Ayache 1989).

The product of the axis $\hat{\boldsymbol{n}}$ and angle θ, $\boldsymbol{\omega} = \theta\hat{\boldsymbol{n}} = (\omega_x, \omega_y, \omega_z)$, is a minimal representation for a 3D rotation. Rotations through common angles such as multiples of $90°$ can be represented exactly (and converted to exact matrices) if θ is stored in degrees. Unfortunately, this representation is not unique, since we can always add a multiple of 360° (2π radians) to θ and get the same rotation matrix. As well, $(\hat{\boldsymbol{n}}, \theta)$ and $(-\hat{\boldsymbol{n}}, -\theta)$ represent the same rotation.

However, for small rotations (e.g., corrections to rotations), this is an excellent choice. In particular, for small (infinitesimal or instantaneous) rotations and θ expressed in radians, Rodriguez's formula simplifies to

$$\boldsymbol{R}(\boldsymbol{\omega}) \approx \boldsymbol{I} + \sin\theta[\hat{\boldsymbol{n}}]_\times \approx \boldsymbol{I} + [\theta\hat{\boldsymbol{n}}]_\times = \begin{bmatrix} 1 & -\omega_z & \omega_y \\ \omega_z & 1 & -\omega_x \\ -\omega_y & \omega_x & 1 \end{bmatrix}, \tag{2.35}$$

which gives a nice linearized relationship between the rotation parameters $\boldsymbol{\omega}$ and $\boldsymbol{R}$. We can also write $\boldsymbol{R}(\boldsymbol{\omega})\boldsymbol{v} \approx \boldsymbol{v} + \boldsymbol{\omega} \times \boldsymbol{v}$, which is handy when we want to compute the derivative of $\boldsymbol{Rv}$ with respect to $\boldsymbol{\omega}$,

$$\frac{\partial \boldsymbol{Rv}}{\partial \boldsymbol{\omega}^T} = -[\boldsymbol{v}]_\times = \begin{bmatrix} 0 & z & -y \\ -z & 0 & x \\ y & -x & 0 \end{bmatrix}. \tag{2.36}$$

Another way to derive a rotation through a finite angle is called the *exponential twist* (Murray, Li, and Sastry 1994). A rotation by an angle θ is equivalent to k rotations through θ/k. In the limit as $k \to \infty$, we obtain

$$\boldsymbol{R}(\hat{\boldsymbol{n}}, \theta) = \lim_{k\to\infty} (\boldsymbol{I} + \frac{1}{k}[\theta\hat{\boldsymbol{n}}]_\times)^k = \exp\,[\boldsymbol{\omega}]_\times. \tag{2.37}$$

If we expand the matrix exponential as a Taylor series (using the identity $[\hat{\boldsymbol{n}}]_\times^{k+2} = -[\hat{\boldsymbol{n}}]_\times^k$, $k > 0$, and again assuming θ is in radians),

$$\begin{aligned} \exp\,[\boldsymbol{\omega}]_\times &= \boldsymbol{I} + \theta[\hat{\boldsymbol{n}}]_\times + \frac{\theta^2}{2}[\hat{\boldsymbol{n}}]_\times^2 + \frac{\theta^3}{3!}[\hat{\boldsymbol{n}}]_\times^3 + \cdots \\ &= \boldsymbol{I} + (\theta - \frac{\theta^3}{3!} + \cdots)[\hat{\boldsymbol{n}}]_\times + (\frac{\theta^2}{2} - \frac{\theta^3}{4!} + \cdots)[\hat{\boldsymbol{n}}]_\times^2 \\ &= \boldsymbol{I} + \sin\theta[\hat{\boldsymbol{n}}]_\times + (1 - \cos\theta)[\hat{\boldsymbol{n}}]_\times^2, \end{aligned} \tag{2.38}$$

which yields the familiar Rodriguez's formula.

Unit quaternions

The unit quaternion representation is closely related to the angle/axis representation. A unit quaternion is a unit length 4-vector whose components can be written as $\boldsymbol{q} = (q_x, q_y, q_z, q_w)$ or $\boldsymbol{q} = (x, y, z, w)$ for short. Unit quaternions live on the unit sphere $\|\boldsymbol{q}\| = 1$ and *antipodal* (opposite sign) quaternions, $\boldsymbol{q}$ and $-\boldsymbol{q}$, represent the same rotation (Figure 2.6). Other than this ambiguity (dual covering), the unit quaternion representation of a rotation is unique. Furthermore, the representation is *continuous*, i.e., as rotation matrices vary continuously, one can find a continuous quaternion representation, although the path on the quaternion sphere may wrap all the way around before returning to the "origin" $\boldsymbol{q}_o = (0, 0, 0, 1)$. For these and other reasons given below, quaternions are a very popular representation for pose and for pose interpolation in computer graphics (Shoemake 1985).

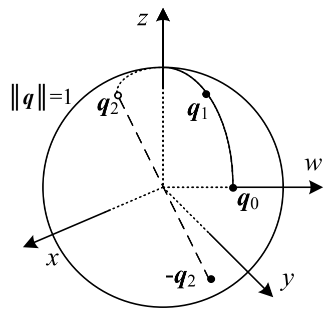

Figure 2.6 Unit quaternions live on the unit sphere $\|\boldsymbol{q}\| = 1$. This figure shows a smooth trajectory through the three quaternions $\boldsymbol{q}_0$, $\boldsymbol{q}_1$, and $\boldsymbol{q}_2$. The *antipodal* point to $\boldsymbol{q}_2$, namely $-\boldsymbol{q}_2$, represents the same rotation as $\boldsymbol{q}_2$.

Quaternions can be derived from the axis/angle representation through the formula

$$\boldsymbol{q} = (\boldsymbol{v}, w) = (\sin\frac{\theta}{2}\hat{\boldsymbol{n}}, \cos\frac{\theta}{2}), \tag{2.39}$$

where $\hat{\boldsymbol{n}}$ and θ are the rotation axis and angle. Using the trigonometric identities $\sin\theta = 2\sin\frac{\theta}{2}\cos\frac{\theta}{2}$ and $(1 - \cos\theta) = 2\sin^2\frac{\theta}{2}$, Rodriguez's formula can be converted to

$$\begin{aligned} \boldsymbol{R}(\hat{\boldsymbol{n}}, \theta) &= \boldsymbol{I} + \sin\theta[\hat{\boldsymbol{n}}]_\times + (1 - \cos\theta)[\hat{\boldsymbol{n}}]^2_\times \\ &= \boldsymbol{I} + 2w[\boldsymbol{v}]_\times + 2[\boldsymbol{v}]^2_\times. \end{aligned} \tag{2.40}$$

This suggests a quick way to rotate a vector $\boldsymbol{v}$ by a quaternion using a series of cross products, scalings, and additions. To obtain a formula for $\boldsymbol{R}(\boldsymbol{q})$ as a function of (x, y, z, w), recall that

$$[\boldsymbol{v}]_\times = \begin{bmatrix} 0 & -z & y \\ z & 0 & -x \\ -y & x & 0 \end{bmatrix} \text{ and } [\boldsymbol{v}]^2_\times = \begin{bmatrix} -y^2 - z^2 & xy & xz \\ xy & -x^2 - z^2 & yz \\ xz & yz & -x^2 - y^2 \end{bmatrix}.$$

We thus obtain

$$\boldsymbol{R}(\boldsymbol{q}) = \begin{bmatrix} 1 - 2(y^2 + z^2) & 2(xy - zw) & 2(xz + yw) \\ 2(xy + zw) & 1 - 2(x^2 + z^2) & 2(yz - xw) \\ 2(xz - yw) & 2(yz + xw) & 1 - 2(x^2 + y^2) \end{bmatrix}. \tag{2.41}$$

The diagonal terms can be made more symmetrical by replacing $1 - 2(y^2 + z^2)$ with $(x^2 + w^2 - y^2 - z^2)$, etc.

The nicest aspect of unit quaternions is that there is a simple algebra for composing rotations expressed as unit quaternions. Given two quaternions $\boldsymbol{q}_0 = (\boldsymbol{v}_0, w_0)$ and $\boldsymbol{q}_1 = (\boldsymbol{v}_1, w_1)$, the *quaternion multiply* operator is defined as

$$\boldsymbol{q}_2 = \boldsymbol{q}_0\boldsymbol{q}_1 = (\boldsymbol{v}_0 \times \boldsymbol{v}_1 + w_0\boldsymbol{v}_1 + w_1\boldsymbol{v}_0,\ w_0w_1 - \boldsymbol{v}_0 \cdot \boldsymbol{v}_1), \tag{2.42}$$

with the property that $\boldsymbol{R}(\boldsymbol{q}_2) = \boldsymbol{R}(\boldsymbol{q}_0)\boldsymbol{R}(\boldsymbol{q}_1)$. Note that quaternion multiplication is *not* commutative, just as 3D rotations and matrix multiplications are not.

procedure *slerp*$(\boldsymbol{q}_0, \boldsymbol{q}_1, \alpha)$:

1. $\boldsymbol{q}_r = \boldsymbol{q}_1/\boldsymbol{q}_0 = (\boldsymbol{v}_r, w_r)$
2. if $w_r < 0$ then $\boldsymbol{q}_r \leftarrow -\boldsymbol{q}_r$
3. $\theta_r = 2\tan^{-1}(\|\boldsymbol{v}_r\|/w_r)$
4. $\hat{\boldsymbol{n}}_r = \mathcal{N}(\boldsymbol{v}_r) = \boldsymbol{v}_r/\|\boldsymbol{v}_r\|$
5. $\theta_\alpha = \alpha\,\theta_r$
6. $\boldsymbol{q}_\alpha = (\sin\frac{\theta_\alpha}{2}\hat{\boldsymbol{n}}_r, \cos\frac{\theta_\alpha}{2})$
7. **return** $\boldsymbol{q}_2 = \boldsymbol{q}_\alpha \boldsymbol{q}_0$

Algorithm 2.1 Spherical linear interpolation (slerp). The axis and total angle are first computed from the quaternion ratio. (This computation can be lifted outside an inner loop that generates a set of interpolated position for animation.) An incremental quaternion is then computed and multiplied by the starting rotation quaternion.

Taking the inverse of a quaternion is easy: Just flip the sign of $\boldsymbol{v}$ or w (but not both!). (You can verify this has the desired effect of transposing the $\boldsymbol{R}$ matrix in (2.41).) Thus, we can also define *quaternion division* as

$$\boldsymbol{q}_2 = \boldsymbol{q}_0/\boldsymbol{q}_1 = \boldsymbol{q}_0\boldsymbol{q}_1^{-1} = (\boldsymbol{v}_0 \times \boldsymbol{v}_1 + w_0\boldsymbol{v}_1 - w_1\boldsymbol{v}_0,\ -w_0w_1 - \boldsymbol{v}_0 \cdot \boldsymbol{v}_1). \tag{2.43}$$

This is useful when the *incremental rotation* between two rotations is desired.

In particular, if we want to determine a rotation that is partway between two given rotations, we can compute the incremental rotation, take a fraction of the angle, and compute the new rotation. This procedure is called *spherical linear interpolation* or *slerp* for short (Shoemake 1985) and is given in Algorithm 2.1. Note that Shoemake presents two formulas other than the one given here. The first exponentiates $\boldsymbol{q}_r$ by alpha before multiplying the original quaternion,

$$\boldsymbol{q}_2 = \boldsymbol{q}_r^\alpha \boldsymbol{q}_0, \tag{2.44}$$

while the second treats the quaternions as 4-vectors on a sphere and uses

$$\boldsymbol{q}_2 = \frac{\sin(1-\alpha)\theta}{\sin\theta}\boldsymbol{q}_0 + \frac{\sin\alpha\theta}{\sin\theta}\boldsymbol{q}_1, \tag{2.45}$$

where $\theta = \cos^{-1}(\boldsymbol{q}_0 \cdot \boldsymbol{q}_1)$ and the dot product is directly between the quaternion 4-vectors. All of these formulas give comparable results, although care should be taken when $\boldsymbol{q}_0$ and $\boldsymbol{q}_1$ are close together, which is why I prefer to use an arctangent to establish the rotation angle.

Which rotation representation is better?

The choice of representation for 3D rotations depends partly on the application.

The axis/angle representation is minimal, and hence does not require any additional constraints on the parameters (no need to re-normalize after each update). If the angle is expressed in degrees, it is easier to understand the pose (say, 90° twist around x-axis), and also easier to express exact rotations. When the angle is in radians, the derivatives of $\boldsymbol{R}$ with respect to $\boldsymbol{\omega}$ can easily be computed (2.36).

Quaternions, on the other hand, are better if you want to keep track of a smoothly moving camera, since there are no discontinuities in the representation. It is also easier to interpolate between rotations and to chain rigid transformations (Murray, Li, and Sastry 1994; Bregler and Malik 1998).

My usual preference is to use quaternions, but to update their estimates using an incremental rotation, as described in Section 6.2.2.

2.1.5 3D to 2D projections

Now that we know how to represent 2D and 3D geometric primitives and how to transform them spatially, we need to specify how 3D primitives are projected onto the image plane. We can do this using a linear 3D to 2D projection matrix. The simplest model is orthography, which requires no division to get the final (inhomogeneous) result. The more commonly used model is perspective, since this more accurately models the behavior of real cameras.

Orthography and para-perspective

An orthographic projection simply drops the z component of the three-dimensional coordinate $\boldsymbol{p}$ to obtain the 2D point $\boldsymbol{x}$. (In this section, we use $\boldsymbol{p}$ to denote 3D points and $\boldsymbol{x}$ to denote 2D points.) This can be written as

$$\boldsymbol{x} = [\boldsymbol{I}_{2\times 2}|\boldsymbol{0}]\,\boldsymbol{p}. \tag{2.46}$$

If we are using homogeneous (projective) coordinates, we can write

$$\tilde{\boldsymbol{x}} = \begin{bmatrix} 1 & 0 & 0 & 0 \\ 0 & 1 & 0 & 0 \\ 0 & 0 & 0 & 1 \end{bmatrix} \tilde{\boldsymbol{p}}, \tag{2.47}$$

i.e., we drop the z component but keep the w component. Orthography is an approximate model for long focal length (telephoto) lenses and objects whose depth is *shallow* relative to their distance to the camera (Sawhney and Hanson 1991). It is exact only for *telecentric* lenses (Baker and Nayar 1999, 2001).

In practice, world coordinates (which may measure dimensions in meters) need to be scaled to fit onto an image sensor (physically measured in millimeters, but ultimately measured in pixels). For this reason, *scaled orthography* is actually more commonly used,

$$\boldsymbol{x} = [s\boldsymbol{I}_{2\times 2}|\boldsymbol{0}]\,\boldsymbol{p}. \tag{2.48}$$

This model is equivalent to first projecting the world points onto a local fronto-parallel image plane and then scaling this image using regular perspective projection. The scaling can be the same for all parts of the scene (Figure 2.7b) or it can be different for objects that are being modeled independently (Figure 2.7c). More importantly, the scaling can vary from frame to frame when estimating *structure from motion*, which can better model the scale change that occurs as an object approaches the camera.

Scaled orthography is a popular model for reconstructing the 3D shape of objects far away from the camera, since it greatly simplifies certain computations. For example, *pose* (camera

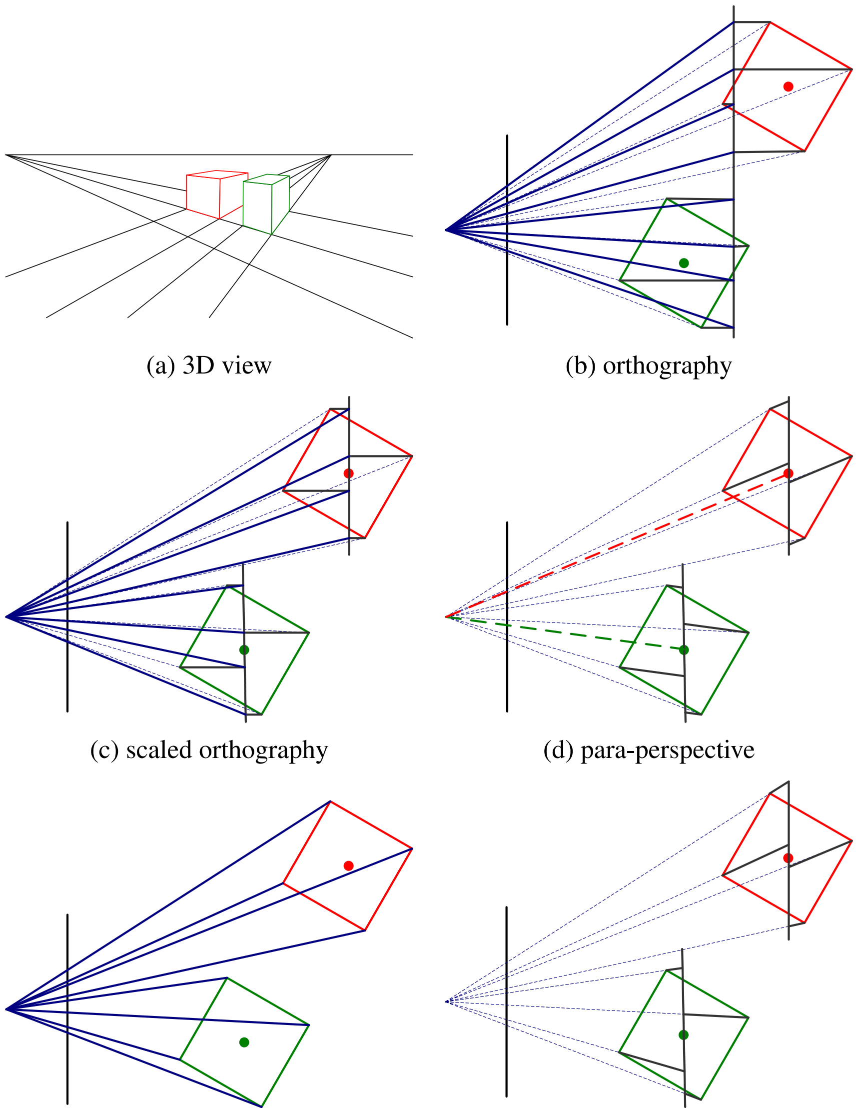

(a) 3D view (b) orthography

(c) scaled orthography (d) para-perspective

(e) perspective (f) object-centered

Figure 2.7 Commonly used projection models: (a) 3D view of world, (b) orthography, (c) scaled orthography, (d) para-perspective, (e) perspective, (f) object-centered. Each diagram shows a top-down view of the projection. Note how parallel lines on the ground plane and box sides remain parallel in the non-perspective projections.

orientation) can be estimated using simple least squares (Section 6.2.1). Under orthography, structure and motion can simultaneously be estimated using *factorization* (singular value decomposition), as discussed in Section 7.3 (Tomasi and Kanade 1992).

A closely related projection model is *para-perspective* (Aloimonos 1990; Poelman and Kanade 1997). In this model, object points are again first projected onto a local reference parallel to the image plane. However, rather than being projected orthogonally to this plane, they are projected *parallel* to the line of sight to the object center (Figure 2.7d). This is followed by the usual projection onto the final image plane, which again amounts to a scaling. The combination of these two projections is therefore *affine* and can be written as

$$\tilde{\boldsymbol{x}} = \begin{bmatrix} a_{00} & a_{01} & a_{02} & a_{03} \\ a_{10} & a_{11} & a_{12} & a_{13} \\ 0 & 0 & 0 & 1 \end{bmatrix} \tilde{\boldsymbol{p}}. \tag{2.49}$$

Note how parallel lines in 3D remain parallel after projection in Figure 2.7b–d. Para-perspective provides a more accurate projection model than scaled orthography, without incurring the added complexity of per-pixel perspective division, which invalidates traditional factorization methods (Poelman and Kanade 1997).

Perspective

The most commonly used projection in computer graphics and computer vision is true 3D *perspective* (Figure 2.7e). Here, points are projected onto the image plane by dividing them by their z component. Using inhomogeneous coordinates, this can be written as

$$\bar{\boldsymbol{x}} = \mathcal{P}_z(\boldsymbol{p}) = \begin{bmatrix} x/z \\ y/z \\ 1 \end{bmatrix}. \tag{2.50}$$

In homogeneous coordinates, the projection has a simple linear form,

$$\tilde{\boldsymbol{x}} = \begin{bmatrix} 1 & 0 & 0 & 0 \\ 0 & 1 & 0 & 0 \\ 0 & 0 & 1 & 0 \end{bmatrix} \tilde{\boldsymbol{p}}, \tag{2.51}$$

i.e., we drop the w component of $\boldsymbol{p}$. Thus, after projection, it is not possible to recover the *distance* of the 3D point from the image, which makes sense for a 2D imaging sensor.

A form often seen in computer graphics systems is a two-step projection that first projects 3D coordinates into *normalized device coordinates* in the range $(x, y, z) \in [-1, -1] \times [-1, 1] \times [0, 1]$, and then rescales these coordinates to integer pixel coordinates using a *viewport* transformation (Watt 1995; OpenGL-ARB 1997). The (initial) perspective projection is then represented using a 4×4 matrix

$$\tilde{\boldsymbol{x}} = \begin{bmatrix} 1 & 0 & 0 & 0 \\ 0 & 1 & 0 & 0 \\ 0 & 0 & -z_{\text{far}}/z_{\text{range}} & z_{\text{near}} z_{\text{far}}/z_{\text{range}} \\ 0 & 0 & 1 & 0 \end{bmatrix} \tilde{\boldsymbol{p}}, \tag{2.52}$$

where z_{near} and z_{far} are the near and far z *clipping planes* and $z_{\text{range}} = z_{\text{far}} - z_{\text{near}}$. Note that the first two rows are actually scaled by the focal length and the aspect ratio so that

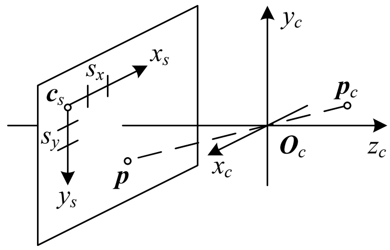

Figure 2.8 Projection of a 3D camera-centered point $\boldsymbol{p}_c$ onto the sensor planes at location $\boldsymbol{p}$. $\boldsymbol{O}_c$ is the camera center (nodal point), $\boldsymbol{c}_s$ is the 3D origin of the sensor plane coordinate system, and s_x and s_y are the pixel spacings.

visible rays are mapped to $(x, y, z) \in [-1, -1]^2$. The reason for keeping the third row, rather than dropping it, is that visibility operations, such as *z-buffering*, require a depth for every graphical element that is being rendered.

If we set $z_{\text{near}} = 1$, $z_{\text{far}} \to \infty$, and switch the sign of the third row, the third element of the normalized screen vector becomes the inverse depth, i.e., the *disparity* (Okutomi and Kanade 1993). This can be quite convenient in many cases since, for cameras moving around outdoors, the inverse depth to the camera is often a more well-conditioned parameterization than direct 3D distance.

While a regular 2D image sensor has no way of measuring distance to a surface point, *range sensors* (Section 12.2) and stereo matching algorithms (Chapter 11) can compute such values. It is then convenient to be able to map from a sensor-based depth or disparity value d directly back to a 3D location using the inverse of a 4×4 matrix (Section 2.1.5). We can do this if we represent perspective projection using a full-rank 4×4 matrix, as in (2.64).

Camera intrinsics

Once we have projected a 3D point through an ideal pinhole using a projection matrix, we must still transform the resulting coordinates according to the pixel sensor spacing and the relative position of the sensor plane to the origin. Figure 2.8 shows an illustration of the geometry involved. In this section, we first present a mapping from 2D pixel coordinates to 3D rays using a sensor homography $\boldsymbol{M}_s$, since this is easier to explain in terms of physically measurable quantities. We then relate these quantities to the more commonly used camera intrinsic matrix $\boldsymbol{K}$, which is used to map 3D camera-centered points $\boldsymbol{p}_c$ to 2D pixel coordinates $\tilde{\boldsymbol{x}}_s$.

Image sensors return pixel values indexed by integer *pixel coordinates* (x_s, y_s), often with the coordinates starting at the upper-left corner of the image and moving down and to the right. (This convention is not obeyed by all imaging libraries, but the adjustment for other coordinate systems is straightforward.) To map pixel centers to 3D coordinates, we first scale the (x_s, y_s) values by the pixel spacings (s_x, s_y) (sometimes expressed in microns for solid-state sensors) and then describe the orientation of the sensor array relative to the camera projection center $\boldsymbol{O}_c$ with an origin $\boldsymbol{c}_s$ and a 3D rotation $\boldsymbol{R}_s$ (Figure 2.8).

The combined 2D to 3D projection can then be written as

$$\boldsymbol{p} = \left[\begin{array}{c|c} \boldsymbol{R}_s & \boldsymbol{c}_s \end{array} \right] \begin{bmatrix} s_x & 0 & 0 \\ 0 & s_y & 0 \\ 0 & 0 & 0 \\ 0 & 0 & 1 \end{bmatrix} \begin{bmatrix} x_s \\ y_s \\ 1 \end{bmatrix} = \boldsymbol{M}_s \bar{\boldsymbol{x}}_s. \tag{2.53}$$

The first two columns of the 3×3 matrix $\boldsymbol{M}_s$ are the 3D vectors corresponding to unit steps in the image pixel array along the x_s and y_s directions, while the third column is the 3D image array origin $\boldsymbol{c}_s$.

The matrix $\boldsymbol{M}_s$ is parameterized by eight unknowns: the three parameters describing the rotation $\boldsymbol{R}_s$, the three parameters describing the translation $\boldsymbol{c}_s$, and the two scale factors (s_x, s_y). Note that we ignore here the possibility of *skew* between the two axes on the image plane, since solid-state manufacturing techniques render this negligible. In practice, unless we have accurate external knowledge of the sensor spacing or sensor orientation, there are only seven degrees of freedom, since the distance of the sensor from the origin cannot be teased apart from the sensor spacing, based on external image measurement alone.

However, estimating a camera model $\boldsymbol{M}_s$ with the required seven degrees of freedom (i.e., where the first two columns are orthogonal after an appropriate re-scaling) is impractical, so most practitioners assume a general 3×3 homogeneous matrix form.

The relationship between the 3D pixel center $\boldsymbol{p}$ and the 3D camera-centered point $\boldsymbol{p}_c$ is given by an unknown scaling s, $\boldsymbol{p} = s\boldsymbol{p}_c$. We can therefore write the complete projection between $\boldsymbol{p}_c$ and a homogeneous version of the pixel address $\tilde{\boldsymbol{x}}_s$ as

$$\tilde{\boldsymbol{x}}_s = \alpha \boldsymbol{M}_s^{-1} \boldsymbol{p}_c = \boldsymbol{K} \boldsymbol{p}_c. \tag{2.54}$$

The 3×3 matrix $\boldsymbol{K}$ is called the *calibration matrix* and describes the camera *intrinsics* (as opposed to the camera's orientation in space, which are called the *extrinsics*).

From the above discussion, we see that $\boldsymbol{K}$ has seven degrees of freedom in theory and eight degrees of freedom (the full dimensionality of a 3×3 homogeneous matrix) in practice. Why, then, do most textbooks on 3D computer vision and multi-view geometry (Faugeras 1993; Hartley and Zisserman 2004; Faugeras and Luong 2001) treat $\boldsymbol{K}$ as an upper-triangular matrix with five degrees of freedom?

While this is usually not made explicit in these books, it is because we cannot recover the full $\boldsymbol{K}$ matrix based on external measurement alone. When calibrating a camera (Chapter 6) based on external 3D points or other measurements (Tsai 1987), we end up estimating the intrinsic $(\boldsymbol{K})$ and extrinsic $(\boldsymbol{R}, \boldsymbol{t})$ camera parameters simultaneously using a series of measurements,

$$\tilde{\boldsymbol{x}}_s = \boldsymbol{K} \left[\begin{array}{c|c} \boldsymbol{R} & \boldsymbol{t} \end{array} \right] \boldsymbol{p}_w = \boldsymbol{P} \boldsymbol{p}_w, \tag{2.55}$$

where $\boldsymbol{p}_w$ are known 3D world coordinates and

$$\boldsymbol{P} = \boldsymbol{K}[\boldsymbol{R}|\boldsymbol{t}] \tag{2.56}$$

is known as the *camera matrix*. Inspecting this equation, we see that we can post-multiply $\boldsymbol{K}$ by $\boldsymbol{R}_1$ and pre-multiply $[\boldsymbol{R}|\boldsymbol{t}]$ by $\boldsymbol{R}_1^T$, and still end up with a valid calibration. Thus, it is impossible based on image measurements alone to know the true orientation of the sensor and the true camera intrinsics.

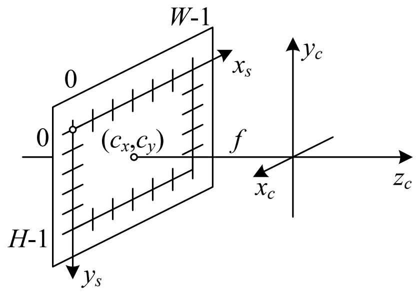

Figure 2.9 Simplified camera intrinsics showing the focal length f and the optical center (c_x, c_y). The image width and height are W and H.

The choice of an upper-triangular form for $\boldsymbol{K}$ seems to be conventional. Given a full 3×4 camera matrix $\boldsymbol{P} = \boldsymbol{K}[\boldsymbol{R}|\boldsymbol{t}]$, we can compute an upper-triangular $\boldsymbol{K}$ matrix using QR factorization (Golub and Van Loan 1996). (Note the unfortunate clash of terminologies: In matrix algebra textbooks, $\boldsymbol{R}$ represents an upper-triangular (right of the diagonal) matrix; in computer vision, $\boldsymbol{R}$ is an orthogonal rotation.)

There are several ways to write the upper-triangular form of $\boldsymbol{K}$. One possibility is

$$\boldsymbol{K} = \begin{bmatrix} f_x & s & c_x \\ 0 & f_y & c_y \\ 0 & 0 & 1 \end{bmatrix}, \tag{2.57}$$

which uses independent *focal lengths* f_x and f_y for the sensor x and y dimensions. The entry s encodes any possible *skew* between the sensor axes due to the sensor not being mounted perpendicular to the optical axis and (c_x, c_y) denotes the *optical center* expressed in pixel coordinates. Another possibility is

$$\boldsymbol{K} = \begin{bmatrix} f & s & c_x \\ 0 & af & c_y \\ 0 & 0 & 1 \end{bmatrix}, \tag{2.58}$$

where the *aspect ratio* a has been made explicit and a common focal length f is used.

In practice, for many applications an even simpler form can be obtained by setting $a = 1$ and $s = 0$,

$$\boldsymbol{K} = \begin{bmatrix} f & 0 & c_x \\ 0 & f & c_y \\ 0 & 0 & 1 \end{bmatrix}. \tag{2.59}$$

Often, setting the origin at roughly the center of the image, e.g., $(c_x, c_y) = (W/2, H/2)$, where W and H are the image height and width, can result in a perfectly usable camera model with a single unknown, i.e., the focal length f.

Figure 2.9 shows how these quantities can be visualized as part of a simplified imaging model. Note that now we have placed the image plane *in front* of the nodal point (projection center of the lens). The sense of the y axis has also been flipped to get a coordinate system compatible with the way that most imaging libraries treat the vertical (row) coordinate. Certain graphics libraries, such as Direct3D, use a left-handed coordinate system, which can lead to some confusion.

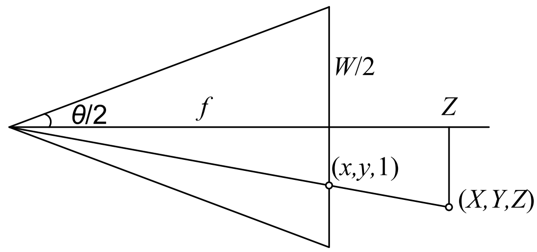

Figure 2.10 Central projection, showing the relationship between the 3D and 2D coordinates, $\boldsymbol{p}$ and $\boldsymbol{x}$, as well as the relationship between the focal length f, image width W, and the field of view θ.

A note on focal lengths

The issue of how to express focal lengths is one that often causes confusion in implementing computer vision algorithms and discussing their results. This is because the focal length depends on the units used to measure pixels.

If we number pixel coordinates using integer values, say $[0, W) \times [0, H)$, the focal length f and camera center (c_x, c_y) in (2.59) can be expressed as pixel values. How do these quantities relate to the more familiar focal lengths used by photographers?

Figure 2.10 illustrates the relationship between the focal length f, the sensor width W, and the field of view θ, which obey the formula

$$\tan\frac{\theta}{2} = \frac{W}{2f} \quad \text{or} \quad f = \frac{W}{2}\left[\tan\frac{\theta}{2}\right]^{-1}. \tag{2.60}$$

For conventional film cameras, $W = 35\text{mm}$, and hence f is also expressed in millimeters. Since we work with digital images, it is more convenient to express W in pixels so that the focal length f can be used directly in the calibration matrix $\boldsymbol{K}$ as in (2.59).

Another possibility is to scale the pixel coordinates so that they go from $[-1, 1)$ along the longer image dimension and $[-a^{-1}, a^{-1})$ along the shorter axis, where $a \geq 1$ is the *image aspect ratio* (as opposed to the *sensor cell aspect ratio* introduced earlier). This can be accomplished using *modified normalized device coordinates*,

$$x'_s = (2x_s - W)/S \text{ and } y'_s = (2y_s - H)/S, \quad \text{where} \quad S = \max(W, H). \tag{2.61}$$

This has the advantage that the focal length f and optical center (c_x, c_y) become independent of the image resolution, which can be useful when using multi-resolution, image-processing algorithms, such as image pyramids (Section 3.5).[2] The use of S instead of W also makes the focal length the same for landscape (horizontal) and portrait (vertical) pictures, as is the case in 35mm photography. (In some computer graphics textbooks and systems, normalized device coordinates go from $[-1, 1] \times [-1, 1]$, which requires the use of two different focal lengths to describe the camera intrinsics (Watt 1995; OpenGL-ARB 1997).) Setting $S = W = 2$ in (2.60), we obtain the simpler (unitless) relationship

$$f^{-1} = \tan\frac{\theta}{2}. \tag{2.62}$$

[2] To make the conversion truly accurate after a downsampling step in a pyramid, floating point values of W and H would have to be maintained since they can become non-integral if they are ever odd at a larger resolution in the pyramid.

The conversion between the various focal length representations is straightforward, e.g., to go from a unitless f to one expressed in pixels, multiply by $W/2$, while to convert from an f expressed in pixels to the equivalent 35mm focal length, multiply by $35/W$.

Camera matrix

Now that we have shown how to parameterize the calibration matrix $\boldsymbol{K}$, we can put the camera intrinsics and extrinsics together to obtain a single 3×4 *camera matrix*

$$\boldsymbol{P} = \boldsymbol{K} \left[\begin{array}{c|c} \boldsymbol{R} & \boldsymbol{t} \end{array} \right]. \tag{2.63}$$

It is sometimes preferable to use an invertible 4×4 matrix, which can be obtained by not dropping the last row in the $\boldsymbol{P}$ matrix,

$$\tilde{\boldsymbol{P}} = \begin{bmatrix} \boldsymbol{K} & \boldsymbol{0} \\ \boldsymbol{0}^T & 1 \end{bmatrix} \begin{bmatrix} \boldsymbol{R} & \boldsymbol{t} \\ \boldsymbol{0}^T & 1 \end{bmatrix} = \tilde{\boldsymbol{K}}\boldsymbol{E}, \tag{2.64}$$

where $\boldsymbol{E}$ is a 3D rigid-body (Euclidean) transformation and $\tilde{\boldsymbol{K}}$ is the full-rank calibration matrix. The 4×4 camera matrix $\tilde{\boldsymbol{P}}$ can be used to map directly from 3D world coordinates $\bar{\boldsymbol{p}}_w = (x_w, y_w, z_w, 1)$ to screen coordinates (plus disparity), $\boldsymbol{x}_s = (x_s, y_s, 1, d)$,

$$\boldsymbol{x}_s \sim \tilde{\boldsymbol{P}}\bar{\boldsymbol{p}}_w, \tag{2.65}$$

where $\sim$ indicates equality up to scale. Note that after multiplication by $\tilde{\boldsymbol{P}}$, the vector is divided by the *third* element of the vector to obtain the normalized form $\boldsymbol{x}_s = (x_s, y_s, 1, d)$.

Plane plus parallax (projective depth)

In general, when using the 4×4 matrix $\tilde{\boldsymbol{P}}$, we have the freedom to remap the last row to whatever suits our purpose (rather than just being the "standard" interpretation of disparity as inverse depth). Let us re-write the last row of $\tilde{\boldsymbol{P}}$ as $\boldsymbol{p}_3 = s_3[\hat{\boldsymbol{n}}_0|c_0]$, where $\|\hat{\boldsymbol{n}}_0\| = 1$. We then have the equation

$$d = \frac{s_3}{z}(\hat{\boldsymbol{n}}_0 \cdot \boldsymbol{p}_w + c_0), \tag{2.66}$$

where $z = \boldsymbol{p}_2 \cdot \bar{\boldsymbol{p}}_w = \boldsymbol{r}_z \cdot (\boldsymbol{p}_w - \boldsymbol{c})$ is the distance of $\boldsymbol{p}_w$ from the camera center C (2.25) along the optical axis Z (Figure 2.11). Thus, we can interpret d as the *projective disparity* or *projective depth* of a 3D scene point $\boldsymbol{p}_w$ from the *reference plane* $\hat{\boldsymbol{n}}_0 \cdot \boldsymbol{p}_w + c_0 = 0$ (Szeliski and Coughlan 1997; Szeliski and Golland 1999; Shade, Gortler, He *et al.* 1998; Baker, Szeliski, and Anandan 1998). (The projective depth is also sometimes called *parallax* in reconstruction algorithms that use the term *plane plus parallax* (Kumar, Anandan, and Hanna 1994; Sawhney 1994).) Setting $\hat{\boldsymbol{n}}_0 = \boldsymbol{0}$ and $c_0 = 1$, i.e., putting the reference plane at infinity, results in the more standard $d = 1/z$ version of disparity (Okutomi and Kanade 1993).

Another way to see this is to invert the $\tilde{\boldsymbol{P}}$ matrix so that we can map pixels plus disparity directly back to 3D points,

$$\tilde{\boldsymbol{p}}_w = \tilde{\boldsymbol{P}}^{-1}\boldsymbol{x}_s. \tag{2.67}$$

In general, we can choose $\tilde{\boldsymbol{P}}$ to have whatever form is convenient, i.e., to sample space using an arbitrary projection. This can come in particularly handy when setting up multi-view

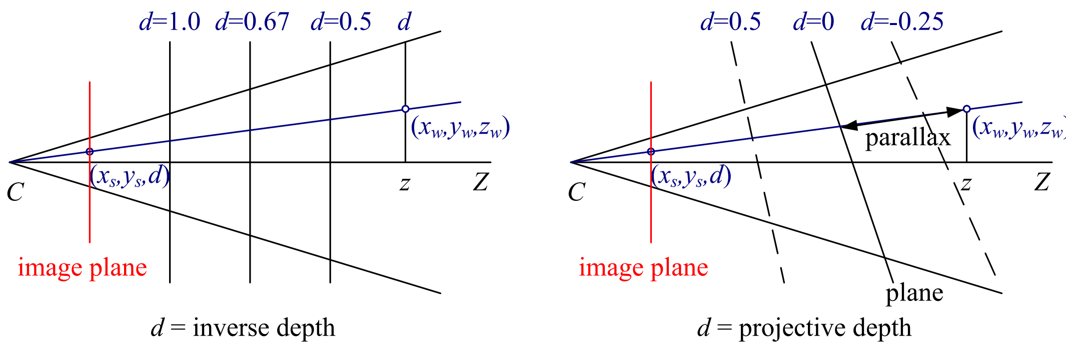

Figure 2.11 Regular disparity (inverse depth) and projective depth (parallax from a reference plane).

stereo reconstruction algorithms, since it allows us to sweep a series of planes (Section 11.1.2) through space with a variable (projective) sampling that best matches the sensed image motions (Collins 1996; Szeliski and Golland 1999; Saito and Kanade 1999).

Mapping from one camera to another

What happens when we take two images of a 3D scene from different camera positions or orientations (Figure 2.12a)? Using the full rank 4×4 camera matrix $\tilde{\boldsymbol{P}} = \tilde{\boldsymbol{K}}\boldsymbol{E}$ from (2.64), we can write the projection from world to screen coordinates as

$$\tilde{\boldsymbol{x}}_0 \sim \tilde{\boldsymbol{K}}_0 \boldsymbol{E}_0 \boldsymbol{p} = \tilde{\boldsymbol{P}}_0 \boldsymbol{p}. \tag{2.68}$$

Assuming that we know the z-buffer or disparity value d_0 for a pixel in one image, we can compute the 3D point location $\boldsymbol{p}$ using

$$\boldsymbol{p} \sim \boldsymbol{E}_0^{-1} \tilde{\boldsymbol{K}}_0^{-1} \tilde{\boldsymbol{x}}_0 \tag{2.69}$$

and then project it into another image yielding

$$\tilde{\boldsymbol{x}}_1 \sim \tilde{\boldsymbol{K}}_1 \boldsymbol{E}_1 \boldsymbol{p} = \tilde{\boldsymbol{K}}_1 \boldsymbol{E}_1 \boldsymbol{E}_0^{-1} \tilde{\boldsymbol{K}}_0^{-1} \tilde{\boldsymbol{x}}_0 = \tilde{\boldsymbol{P}}_1 \tilde{\boldsymbol{P}}_0^{-1} \tilde{\boldsymbol{x}}_0 = \boldsymbol{M}_{10} \tilde{\boldsymbol{x}}_0. \tag{2.70}$$

Unfortunately, we do not usually have access to the depth coordinates of pixels in a regular photographic image. However, for a *planar scene*, as discussed above in (2.66), we can replace the last row of $\boldsymbol{P}_0$ in (2.64) with a general *plane equation*, $\hat{\boldsymbol{n}}_0 \cdot \boldsymbol{p} + c_0$ that maps points on the plane to $d_0 = 0$ values (Figure 2.12b). Thus, if we set $d_0 = 0$, we can ignore the last column of $\boldsymbol{M}_{10}$ in (2.70) and also its last row, since we do not care about the final z-buffer depth. The mapping equation (2.70) thus reduces to

$$\tilde{\boldsymbol{x}}_1 \sim \tilde{\boldsymbol{H}}_{10} \tilde{\boldsymbol{x}}_0, \tag{2.71}$$

where $\tilde{\boldsymbol{H}}_{10}$ is a general 3×3 homography matrix and $\tilde{\boldsymbol{x}}_1$ and $\tilde{\boldsymbol{x}}_0$ are now 2D homogeneous coordinates (i.e., 3-vectors) (Szeliski 1996).This justifies the use of the 8-parameter homography as a general alignment model for mosaics of planar scenes (Mann and Picard 1994; Szeliski 1996).

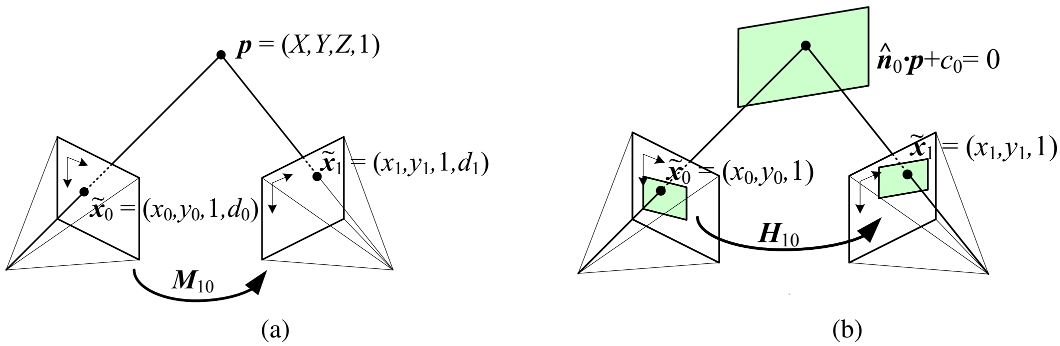

Figure 2.12 A point is projected into two images: (a) relationship between the 3D point coordinate $(X, Y, Z, 1)$ and the 2D projected point $(x, y, 1, d)$; (b) planar homography induced by points all lying on a common plane $\hat{\boldsymbol{n}}_0 \cdot \boldsymbol{p} + c_0 = 0$.

The other special case where we do not need to know depth to perform inter-camera mapping is when the camera is undergoing pure rotation (Section 9.1.3), i.e., when $\boldsymbol{t}_0 = \boldsymbol{t}_1$. In this case, we can write

$$\tilde{\boldsymbol{x}}_1 \sim \boldsymbol{K}_1 \boldsymbol{R}_1 \boldsymbol{R}_0^{-1} \boldsymbol{K}_0^{-1} \tilde{\boldsymbol{x}}_0 = \boldsymbol{K}_1 \boldsymbol{R}_{10} \boldsymbol{K}_0^{-1} \tilde{\boldsymbol{x}}_0, \tag{2.72}$$

which again can be represented with a 3×3 homography. If we assume that the calibration matrices have known aspect ratios and centers of projection (2.59), this homography can be parameterized by the rotation amount and the two unknown focal lengths. This particular formulation is commonly used in image-stitching applications (Section 9.1.3).

Object-centered projection

When working with long focal length lenses, it often becomes difficult to reliably estimate the focal length from image measurements alone. This is because the focal length and the distance to the object are highly correlated and it becomes difficult to tease these two effects apart. For example, the change in scale of an object viewed through a zoom telephoto lens can either be due to a zoom change or a motion towards the user. (This effect was put to dramatic use in some of Alfred Hitchcock's film *Vertigo*, where the simultaneous change of zoom and camera motion produces a disquieting effect.)

This ambiguity becomes clearer if we write out the projection equation corresponding to the simple calibration matrix $\boldsymbol{K}$ (2.59),

$$x_s = f \frac{\boldsymbol{r}_x \cdot \boldsymbol{p} + t_x}{\boldsymbol{r}_z \cdot \boldsymbol{p} + t_z} + c_x \tag{2.73}$$

$$y_s = f \frac{\boldsymbol{r}_y \cdot \boldsymbol{p} + t_y}{\boldsymbol{r}_z \cdot \boldsymbol{p} + t_z} + c_y, \tag{2.74}$$

where $\boldsymbol{r}_x$, $\boldsymbol{r}_y$, and $\boldsymbol{r}_z$ are the three rows of $\boldsymbol{R}$. If the distance to the object center $t_z \gg \|\boldsymbol{p}\|$ (the size of the object), the denominator is approximately t_z and the overall scale of the projected object depends on the ratio of f to t_z. It therefore becomes difficult to disentangle these two quantities.

To see this more clearly, let $\eta_z = t_z^{-1}$ and $s = \eta_z f$. We can then re-write the above equations as

$$x_s = s\frac{\boldsymbol{r}_x \cdot \boldsymbol{p} + t_x}{1 + \eta_z \boldsymbol{r}_z \cdot \boldsymbol{p}} + c_x \tag{2.75}$$

$$y_s = s\frac{\boldsymbol{r}_y \cdot \boldsymbol{p} + t_y}{1 + \eta_z \boldsymbol{r}_z \cdot \boldsymbol{p}} + c_y \tag{2.76}$$

(Szeliski and Kang 1994; Pighin, Hecker, Lischinski *et al.* 1998). The scale of the projection s can be reliably estimated if we are looking at a known object (i.e., the 3D coordinates $\boldsymbol{p}$ are known). The inverse distance η_z is now mostly decoupled from the estimates of s and can be estimated from the amount of *foreshortening* as the object rotates. Furthermore, as the lens becomes longer, i.e., the projection model becomes orthographic, there is no need to replace a perspective imaging model with an orthographic one, since the same equation can be used, with $\eta_z \to 0$ (as opposed to f and t_z both going to infinity). This allows us to form a natural link between orthographic reconstruction techniques such as factorization and their projective/perspective counterparts (Section 7.3).

2.1.6 Lens distortions

The above imaging models all assume that cameras obey a *linear* projection model where straight lines in the world result in straight lines in the image. (This follows as a natural consequence of linear matrix operations being applied to homogeneous coordinates.) Unfortunately, many wide-angle lenses have noticeable *radial distortion*, which manifests itself as a visible curvature in the projection of straight lines. (See Section 2.2.3 for a more detailed discussion of lens optics, including chromatic aberration.) Unless this distortion is taken into account, it becomes impossible to create highly accurate photorealistic reconstructions. For example, image mosaics constructed without taking radial distortion into account will often exhibit blurring due to the mis-registration of corresponding features before pixel blending (Chapter 9).

Fortunately, compensating for radial distortion is not that difficult in practice. For most lenses, a simple quartic model of distortion can produce good results. Let (x_c, y_c) be the pixel coordinates obtained *after* perspective division but *before* scaling by focal length f and shifting by the optical center (c_x, c_y), i.e.,

$$\begin{aligned} x_c &= \frac{\boldsymbol{r}_x \cdot \boldsymbol{p} + t_x}{\boldsymbol{r}_z \cdot \boldsymbol{p} + t_z} \\ y_c &= \frac{\boldsymbol{r}_y \cdot \boldsymbol{p} + t_y}{\boldsymbol{r}_z \cdot \boldsymbol{p} + t_z}. \end{aligned} \tag{2.77}$$

The radial distortion model says that coordinates in the observed images are displaced away (*barrel* distortion) or towards (*pincushion* distortion) the image center by an amount proportional to their radial distance (Figure 2.13a–b).[3] The simplest radial distortion models use low-order polynomials, e.g.,

$$\begin{aligned} \hat{x}_c &= x_c(1 + \kappa_1 r_c^2 + \kappa_2 r_c^4) \\ \hat{y}_c &= y_c(1 + \kappa_1 r_c^2 + \kappa_2 r_c^4), \end{aligned} \tag{2.78}$$

[3] Anamorphic lenses, which are widely used in feature film production, do not follow this radial distortion model. Instead, they can be thought of, to a first approximation, as inducing different vertical and horizontal scalings, i.e., non-square pixels.

(a) (b) (c)

Figure 2.13 Radial lens distortions: (a) barrel, (b) pincushion, and (c) fisheye. The fisheye image spans almost 180° from side-to-side.

where $r_c^2 = x_c^2 + y_c^2$ and κ_1 and κ_2 are called the *radial distortion parameters*.[4] After the radial distortion step, the final pixel coordinates can be computed using

$$\begin{aligned} x_s &= f x'_c + c_x \\ y_s &= f y'_c + c_y. \end{aligned} \tag{2.79}$$

A variety of techniques can be used to estimate the radial distortion parameters for a given lens, as discussed in Section 6.3.5.

Sometimes the above simplified model does not model the true distortions produced by complex lenses accurately enough (especially at very wide angles). A more complete analytic model also includes *tangential distortions* and *decentering distortions* (Slama 1980), but these distortions are not covered in this book.

Fisheye lenses (Figure 2.13c) require a model that differs from traditional polynomial models of radial distortion. Fisheye lenses behave, to a first approximation, as *equi-distance* projectors of angles away from the optical axis (Xiong and Turkowski 1997), which is the same as the *polar projection* described by Equations (9.22–9.24). Xiong and Turkowski (1997) describe how this model can be extended with the addition of an extra quadratic correction in ϕ and how the unknown parameters (center of projection, scaling factor s, etc.) can be estimated from a set of overlapping fisheye images using a direct (intensity-based) non-linear minimization algorithm.

For even larger, less regular distortions, a parametric distortion model using splines may be necessary (Goshtasby 1989). If the lens does not have a single center of projection, it may become necessary to model the 3D *line* (as opposed to *direction*) corresponding to each pixel separately (Gremban, Thorpe, and Kanade 1988; Champleboux, Lavallée, Sautot *et al.* 1992; Grossberg and Nayar 2001; Sturm and Ramalingam 2004; Tardif, Sturm, Trudeau *et al.* 2009). Some of these techniques are described in more detail in Section 6.3.5, which discusses how to calibrate lens distortions.

[4] Sometimes the relationship between x_c and $\hat{x}_c$ is expressed the other way around, i.e., $x_c = \hat{x}_c(1 + \kappa_1 \hat{r}_c^2 + \kappa_2 \hat{r}_c^4)$. This is convenient if we map image pixels into (warped) rays by dividing through by f. We can then undistort the rays and have true 3D rays in space.

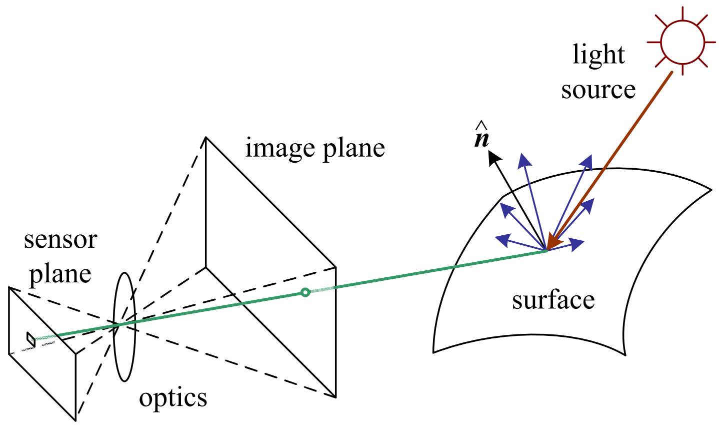

Figure 2.14 A simplified model of photometric image formation. Light is emitted by one or more light sources and is then reflected from an object's surface. A portion of this light is directed towards the camera. This simplified model ignores multiple reflections, which often occur in real-world scenes.

There is one subtle issue associated with the simple radial distortion model that is often glossed over. We have introduced a non-linearity between the perspective projection and final sensor array projection steps. Therefore, we cannot, in general, post-multiply an arbitrary 3×3 matrix $\boldsymbol{K}$ with a rotation to put it into upper-triangular form and absorb this into the global rotation. However, this situation is not as bad as it may at first appear. For many applications, keeping the simplified diagonal form of (2.59) is still an adequate model. Furthermore, if we correct radial and other distortions to an accuracy where straight lines are preserved, we have essentially converted the sensor back into a linear imager and the previous decomposition still applies.

2.2 Photometric image formation

In modeling the image formation process, we have described how 3D geometric features in the world are projected into 2D features in an image. However, images are not composed of 2D features. Instead, they are made up of discrete color or intensity values. Where do these values come from? How do they relate to the lighting in the environment, surface properties and geometry, camera optics, and sensor properties (Figure 2.14)? In this section, we develop a set of models to describe these interactions and formulate a generative process of image formation. A more detailed treatment of these topics can be found in other textbooks on computer graphics and image synthesis (Glassner 1995; Weyrich, Lawrence, Lensch *et al.* 2008; Foley, van Dam, Feiner *et al.* 1995; Watt 1995; Cohen and Wallace 1993; Sillion and Puech 1994).

2.2.1 Lighting

Images cannot exist without light. To produce an image, the scene must be illuminated with one or more light sources. (Certain modalities such as fluorescent microscopy and X-ray